Patterns, Forces, and Metastable Pathways in Debonding of Elastic Films

Jayati Sarkar,[1] Vijay Shenoy,[2,*] and Ashutosh Sharma[1,†]
[1]*Chemical Engineering Department, Indian Institute of Technology Kanpur, UP 208 016, India*
[2]*Material Research Centre, Indian Institute of Science, Bangalore 560 012, India*
(Received 20 October 2003; published 30 June 2004)

This Letter resolves several intriguing and fundamental aspects of debonding at soft interfaces, including the formation and persistence of regularly arranged nanocavities and bridges, "adhesion-debonding hysteresis," and vastly lower adhesive strengths compared to the absence of pattern formation. The analysis shows the hysteresis to be caused by an energy barrier that separates the metastable patterned configuration during withdrawal, and the debonded state. The metastable morphological pathways involving cavitation and peeling of contact zones engender substantially lower debonding forces.

DOI: 10.1103/PhysRevLett.93.018302 PACS numbers: 82.35.Gh, 68.35.Ct, 68.55.–a

The related phenomena of adhesion, debonding, and interfacial cavitation at soft interfaces have been intensely studied both for their technological applications and for many unresolved scientific issues [1–10]. A rigid contactor, initially in contact with a soft elastic film, debonds upon withdrawal by the formation of a pattern consisting of areas of intimate contact and interfacial cavities of well defined spacing [1–4]. The length scale of this pattern depends linearly on the film thickness, but is independent of the adhesive strength and the elastic properties of the film [2,4]. Despite a clear appreciation of the central role played by interfacial cavitation in debonding and tackiness [7,8], the theoretical understanding of its origin, its persistence, and the mechanisms by which it influences the debonding has remained incomplete. Cavitation may arise from a host of complexities such as contactor surface roughness [7], nucleation from defects (this mechanism is absent in incompressible films), and a rate dependent continuous nucleation proposed to be operative in viscoelastic materials [8]. *We consider here the case of a smooth flat contactor and an incompressible, purely elastic film rigidly bonded to a substrate as the most basic model.* These conditions are indeed closely met in the recent experiments [2–4] we address. Another recent attempt at an explanation of nonrandomly distributed cavities in such systems is based on a linear stability analysis [5] that showed spontaneous surface roughening due to the lowering of the system energy when the contactor approaches the film to within a small critical distance ($d_c < 10$ nm). The main unresolved point, however, is that this spontaneously patterned state persists upon withdrawal much beyond d_c, where the energy considerations (and the linear analysis) predict its disappearance. This difference between approach and withdrawal behaviors engendered by cavitation may be referred to as "adhesion debonding" or "contact hysteresis." Although adhesion hysteresis arising from viscoelasticity, dissipation, and changes in material and interfacial properties [10] is undoubtedly significant depending on the materials used, we show here that contact hysteresis is, in fact, fundamental to debonding of elastic interfaces even in the absence of time dependent changes and flow. Another unresolved issue addressed here is the role of cavities in reducing the pull-off force required for debonding, which can be several orders smaller [3] than the force calculated based on the assumption of flat surfaces. Clearly, such a significant reduction cannot be explained merely by ~50% reduction in the contact area observed at detachment [3]. Here we consider the above issues of patterned interfacial cavity formation and persistence upon contactor withdrawal, its associated morphologies, and the pull-off force and pull-off distance as the key unresolved issues in debonding of a purely elastic film from a flat, smooth, and rigid surface.

Figure 1 illustrates the laterally unconfined elastic film—smooth contactor geometry in a plane strain configuration. The total energy consists of the stabilizing stored elastic energy and the destabilizing attractive interaction between the contactor and the film.

$$\Pi = \int_V W(\boldsymbol{\epsilon}) dV + \int_S U(d_0 - \boldsymbol{u}\cdot\boldsymbol{n}) dS, \qquad (1)$$

where W is the strain energy density defined as $W(\boldsymbol{\epsilon}) = \frac{1}{2}\mu(\boldsymbol{\epsilon}:\boldsymbol{\epsilon})$ (where $\boldsymbol{\epsilon}$ is the strain tensor), $\boldsymbol{u}$ is the displacement vector, and μ is the shear modulus of the film ($\lesssim 10$ MPa). The interaction potential consists of an attractive van der Waals component along with a short

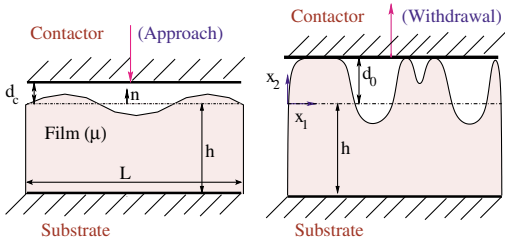

FIG. 1 (color online). Left: Schematic of small amplitude pattern formation on approach at critical distance d_c in a laterally unconfined film. Right: Column stretching and growth of cavities on withdrawal of the contactor.

range Born repulsion, represented by $U(d_0 - \boldsymbol{u}\cdot\boldsymbol{n}) = -A/12\pi(d_0 - \boldsymbol{u}\cdot\boldsymbol{n})^2 + B/(d_0 - \boldsymbol{u}\cdot\boldsymbol{n})^8$, where A is the Hamaker constant (of the order of 10^{-20} J) and B is the coefficient of Born repulsion. The coefficient B is correlated to the adhesive energy at contact [$\Delta G = U(d_e) = A/(16\pi d_e^2)$], where d_e is the equilibrium separation distance obtained from $U'(d_e) = 0$. This form of interaction implies that the force required to pull off two rigid flat surfaces is $F_m^f = \Delta G/d_e$. Upon the approach to contact ($d < 10$ nm), the condition for instability $h|U''|/\mu \geq 6.22$ is met and the film surface develops periodic roughness on the length scale ($\lambda \sim 3h$) [5]. How does this length scale persist even when the contactor is pulled back much beyond d_c, as observed experimentally [2–4]?

The adhesion-debonding hysteresis is explained by a simple analysis. For a single Fourier mode, $u_2(x) = a_k \cos kx$, the total energy (per unit length of the film) is shown in Fig. 2 for two different values of the gap thickness d_0 above and below the critical distance d_c. The patterned configuration with $hk \approx 2.12$ has the lowest energy for $d_0 < d_c$ rather than flat film [5]. However, for $d_0 > d_c$, the flat film configuration has the lower energy, although the patterned state remains a *local* minimum, metastable state. For $d_0 > d_c$, the global (flat) and the local (patterned) minima are separated by a large energy barrier (Fig. 2). *It is due to the presence of this energy barrier that the patterned state formed during the approach persists in its metastable configuration upon withdrawal.* Indeed, the pattern is far more complex with many Fourier modes, leading to a multiplicity of metastable states of varying energies. Thus, during the pull off, the system "hops" through a succession of metastable states leading to a strong "path dependence" especially in the presence of heterogeneities, noise, etc.

The complete simulation of the pull-off process is achieved by the Fourier representation $u_2(x_1, 0) = \sum_{n=0}^{N-1} a_n \cos(k_n x_1)$, where a_n is the amplitude of the nth Fourier mode with wave number $k_n (= 2\pi n/L)$. The total energy per unit depth of the film

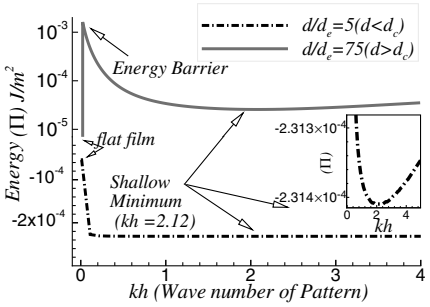

FIG. 2. Energy landscape as a function of wave number. The plots show the presence of an energy barrier separating the flat film and patterned state for large values of d_0/d_e. The physical parameters are $\mu = 0.1$ MPa, $h = 10$ μm, $A = 10^{-20}$ J, $\Delta G = 1.0$ mJ/m^2. Inset magnifies the minimum.

$$\Pi = \pi\mu L \sum_{n=0}^{N-1} n a_n^2 k_n S(k_n h)/2 + \int_0^L U(d_0 - u_2) dx_1. \quad (2)$$

The stresses that develop in the film are determined from the Fourier coefficients as $\sigma_{22}(x_1, 0) = 2\mu \sum_{n=0}^{N-1} \times a_n k_n S(k_n h) \cos k_n x_1$, where $S(\xi) = \frac{1+\cosh(2\xi)+2\xi^2}{\sinh(2\xi)-2\xi}$ [5]. F is the average force per unit area exerted on the contactor plate to maintain equilibrium at a given separation.

A conjugate gradient (CG) scheme (which finds the local minimum closest to the initial configuration) was employed to find the Fourier coefficients that result in a minimum energy pattern for a given separation distance. Simulations started by reducing the distance below d_c (approach) are followed by retraction (withdrawal). The separation distance was changed in steps of s, taking the energy minimizing pattern of the previous step as the initial state in the CG scheme. To uncover the range of possible metastable pathways, we varied the step size s and, in addition, have considered cases where the energy minimizing Fourier coefficients (at d_0) are perturbed randomly before being taken as initial choices for the next step. The perturbations are introduced by multiplying each Fourier coefficient with $(1 + r)$ where r is a random number between $-\epsilon$ and ϵ, where ϵ is called the noise amplitude.

Figure 3(a) depicts typical changes in the film morphology during the process of pull off starting from the critical distance d_c where the instability originates. This simulation (without noise) shows the columns/cavities being laterally separated by $\sim 3h$ at all separation distances until the maximum force is reached. Thus, the initial nanocavities formed at the contact proximity ($d < d_c$) persist during pull off. Figures 3(b) and 3(c) show, respectively, the variation of fractional contact area ($\alpha =$ area of contacts/total film surface area) and the force F on the contactor, with gap thickness for different step sizes. For small step sizes ($\lesssim 0.3$ nm) the debonding pathway is such that the configuration is trapped in the energy minimum corresponding to the initial instability. The contact area remains constant and the force increases almost linearly until a catastrophic snap-off of the bridging columns. Remarkably, the maximum force F_m that can be sustained before debonding is about an order of magnitude smaller than the maximum adhesive force F_m^f. The formation of bridges and cavities allows very high concentration of elastic stresses near the edges of the columns. For small step sizes, the elastic stresses build up to very high levels comparable to the maximum adhesive force, without any intermediate small relaxations, since the structure is trapped in the original deep energy minimum. This engenders a catastrophic adhesive failure for small step sizes. In contrast, larger step sizes force the structure to hop through a succession of metastable states with lower barrier heights releasing energy intermittently, leading to a continuous decrease in the contact area. The stresses at the edges of the contacts are not large

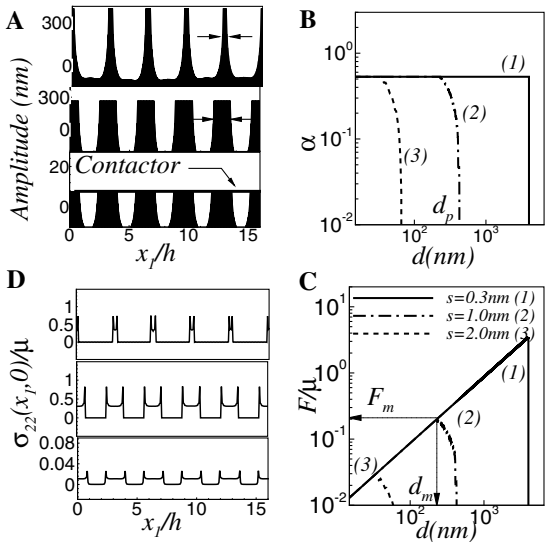

FIG. 3. (a) Film profiles at various separation distances without external noise and step size of 1 nm ($A = 10^{-20}$ J, $\mu =$ 0.5 MPa, $h = 10$ μm). (b),(c) Variation, respectively, of fractional contact area α and force F/μ with separation distances: Curves (1), (2), and (3) correspond to the step sizes of 0.3, 1, and 2 nm, respectively. Curves (1) and (3) correspond to the catastrophic column collapse and continuous peeling modes of failure, and curve (2) is an intermediate. (d) Normal stress distribution along the surface of the film for cases in (a) showing maximum stresses, responsible for peeling, at the column edges.

enough to cause catastrophic detachment, but are sufficient to sustain peeling. For intermediate step sizes [curve (2) of Fig. 3(b)], the initial phase of pulling reproduces the features of small step size results, followed by the large step size behavior. The escape from the initial high barrier state occurs only after some stretching of columns leading the release of pent-up elastic energy. The ascending branch (''elastic branch'') of the force curve Fig. 3(c) reflects the linear increase of elastic stresses in the columns without any change in the contact area. The initiation of peeling limits the maximum force, after which it declines (''release branch'') with a further increase in the separation distance and a concurrent reduction in the contact area.

A particularly simple model, containing the key physics of the linear decrease of the area, approximates the total energy as $\frac{3}{2}\mu u^2[\alpha/(1-\alpha)h] + \alpha U(d_0 - u)$ where α is the fractional contact area. For a given d_0, the minimum of energy occurs when the fractional contact area is $\alpha(d_0) \approx 1 - [3\mu/2h|U(d_e)|]^{1/2}d_0$. This linear decrease in the contact area with increased separation shows that debonding, even by the application of a purely normal force, actually proceeds by *peeling off the contacts* which requires a much smaller force as compared to homogeneous debonding of flat contact areas.

Although the peeling mode remains the dominant mode of debonding for small levels of noise, another pathway of debonding in the form of cavitation within the contact area leading to column splitting also appears for high noise amplitudes [Fig. 4(a)], i.e., starting from initial conditions that are far from the solution branch being followed in the absence of noise. The column splitting mode is favored for higher adhesive strength and for more compliant films (higher value of $\Delta G h/\mu$) where even smaller amounts of noise can induce this transition. Column splitting, when it occurs, results in a precipitous decrease in the force, usually followed by a regime of nearly constant force [Fig. 4(b)]. Continuous peeling from the sides of the split columns prevents the buildup of elastic force in this regime. This helps understand experimental observations of the constant force regime, which becomes more prominent on rough surfaces that allow cavity initiation within the contact zones [6,7]. Figure 5(a) shows the influence of the initial distance (or the fractional contact area) at which withdrawal is initiated. As expected, a more intimate initial contact engenders a higher pull-off force of similar order of magnitude.

The maximum pull-off distance was obtained for a wide range of parameters $h \sim 0.1$–10 μm, $A \sim 10^{-19}$–10^{-21} J, and $\mu \sim 0.1$–10 MPa; initial $\alpha \sim 0.5$–0.95, step sizes ($s \sim 0.01$–2.0) nm, noise amplitude ($\epsilon \sim 0.001$–0.01), and $\Delta G \sim 1$–100 mJ/m^2. Interestingly, the dependence of the pull-off distance d_p on ΔG, μ, and h is represented by a master curve of the form Fig. 5(b),

$$d_p/d_e \sim (\Delta G h/\mu d_e^2)^p, \tag{3}$$

where the nondimensional parameter $(\Delta G/d_e^2)/(\mu/h)$ is the ratio of the stiffness of the interaction potential and the elastic stiffness of the film. The exponent p is close to 1 for noiseless cases with a small step size and decreases with an increasing step size as well as an increasing level of noise, but p is remarkably independent of the initial contact area [Fig. 5(a)]. As argued earlier, increased step size and noise levels can induce debonding at a smaller distance by cascading through higher energy metastable states. For a given α, the distance at which force is

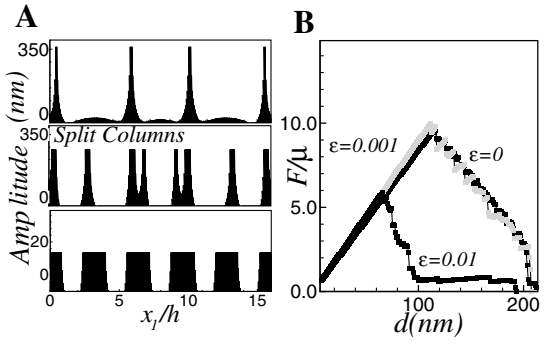

FIG. 4. (a) Noise-induced, column-splitting pathway of adhesive failure for a more strongly adherent film (same as Fig. 3 except $A = 10^{-19}$ J and $\epsilon = 0.01$). (b) Variation of force F/μ with separation distances for various levels of noise ($\epsilon = 0.0, 0.001, 0.01$).

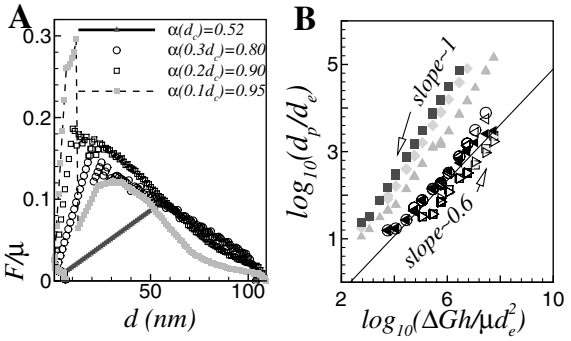

FIG. 5. (a) Variation of F/μ starting with different initial fractional contact area, α ($A = 10^{-20}$ J, $h = 5.0$ μm, $\mu =$ 1.0 MPa, $s = 1$ nm, $\epsilon = 0$, $d_c = 5.4$ nm). (b) Variation of snap-off distance with nondimensional stiffness ratio. The uppermost curve (slope ~1.0) is for the smallest step size, $s =$ 0.01 nm. For the remaining curves, the slope decreases with increased step size and noise ($s = 0.1$–2 nm; $\epsilon = 0$–0.01).

maximum, d_m, was found to scale linearly with the pull-off distance, d_p, where $F \to 0$.

Further, the maximum force was found to scale as

$$F_m h/\mu d_e = C(\Delta G h/\mu d_e^2)^{\delta}. \quad (4)$$

Interestingly, $\delta = 0.55 \pm 0.05$ when the withdrawal is initiated from intimate contact (initial $\alpha > 0.8$; $\epsilon =$ 0–0.01; $s \sim 1$–2 nm). Since experiments are usually done in this regime, simulations indeed support the frequently observed scaling, $F_m \sim (\Delta G \mu/h)^{0.5}$ [3]. However, for small steps ($s \lesssim 0.3$) and low noise, δ can increase to a maximum of 0.8 ± 0.18, especially when the withdrawal is initiated near d_c ($\alpha = 0.5$). In general $\delta \in (0.5, 1)$ was found to decrease with increased step size, noise, and initial contact area. For example, $\delta = 0.48$, 0.51, 0.80, and 0.98, respectively, for the following parameters (α, s, ϵ): (0.5, 0.3, 0.01), (0.8, 2, 0), (0.5, 2, 0), and (0.5, 0.3, 0). The prefactor, C, is in the range of 0.01 to 1.0, such that the force decreases with increased step size and noise, and decreased initial contact area. The above considerations also explain the contention that the surface energy of soft solids as measured from debonding experiments is a nonequilibrium and nonunique property depending on the initial state (light vs intimate contact), defects, vibrations, contactor roughness, etc.

The values of the maximum force per unit area required for debonding are much smaller than predicted for debonding for flat surfaces ($F_m^f \sim \Delta G/d_e$). For example, with $A = 10^{-20}$ J, $h = 10.0$ μm, $\mu = 0.5$ MPa; $F_m^f =$ 80 MPa; $F_m = 0.1$ MPa for $s = 1$ nm, $\epsilon = 0$, $\alpha = 0.53$; $F_m = 0.04$ MPa with $\epsilon = 0.01$; $F_m = 0.2$ MPa for $s =$ 1 nm, $\epsilon = 0$, $\alpha = 0.9$ (intimate contact). The ratio $F_m/F_m^f \sim C(\mu d_e^2/\Delta G h)^{1-\delta}$. This shows that the discrepancy in the forces between the flat and instability controlled modes of failure increases with decreasing shear modulus, increasing adhesive strength and film thickness. Experiments on elastic films show the same force-displacement features [3,7] as in [Fig. 4(b) and 5(a)] and the order of maximum force as in (4). For example, observed $F_m = 2500$ Pa compares with the simulation value of 2632 Pa ($s = 1$ nm) for $h = 100$ μm, $\mu =$ 100 Pa, $\Delta G \sim 120$ mJ/m^2 [3].

This Letter resolves important open questions regarding the mechanisms and pathways of debonding at soft elastic interfaces. The main results include (a) the physical origins of the adhesion-debonding hysteresis (in a purely elastic system), (b) the formation and persistence of regularly arranged cavities and bridges during debonding, (c) the metastable pathways of debonding such as column collapse, column peeling, and column splitting that require much larger pull-off distances and much smaller debonding forces as compared to flat surfaces, and (d) the dependence of pull-off distance and force on adhesion energy, shear modulus, and film thickness. Formation of cavities engenders extremely high stresses near the column edges leading to the peeling of contact zones at much smaller average stresses than the adhesive strength. This is analogous to defects (dislocations and cracks) in solids that give rise to observed yield stress and strength much smaller than ideal values.

Discussions with M. K. Chaudhury and A. Ghatak are gratefully acknowledged. V. S. and A. S. acknowledge DST, India (Nanoscience Program) for support.

*Electronic address: shenoy@mrc.iisc.ernet.in
†Electronic address: ashutos@iitk.ac.in

[1] Y. Y. Lin, C.-Y. Hui, and H. D. Conway, J. Polym. Sci., Pt. B: Polym. Phys. **38**, 2769 (2000).
[2] A. Ghatak, M. K. Chaudhury, V. Shenoy, and A. Sharma, Phys. Rev. Lett. **85**, 4329 (2000); A. Ghatak and M. K. Chaudhury, Langmuir **19**, 2621 (2003).
[3] K. R. Shull, C. M. Flanigan, and A. J. Crosby, Phys. Rev. Lett. **84**, 3057 (2000); C. Creton, J. Hooker, and K. R. Shull, Langmuir **17**, 4948 (2001); R. E. Webber, K. R. Shull, A. Roos, and C. Creton, Phys. Rev. E **68**, 021805 (2003).
[4] W. Mönch and S. Herminghaus, Europhys. Lett. **53**, 525 (2001).
[5] V. Shenoy and A. Sharma, Phys. Rev. Lett. **86**, 119 (2001); J. Mech. Phys. Solids **50**, 1155 (2002); Langmuir **18**, 2216 (2002); C. Q. Ru, J. Appl. Mech. **69**, 97 (2002).
[6] A. Chiche, P. Pareige, and C. Creton, C.R. Acad. Sci. IV Phys. **1**, 1197 (2000).
[7] C. Gay and L. Leibler, Phys. Rev. Lett. **82**, 936 (1999).
[8] I. Chikina and C. Gay, Phys. Rev. Lett. **85**, 4546 (2000).
[9] A. N. Gent and R. P. Petrich, Proc. R. Soc. London, Ser. A **310**, 433 (1969).
[10] M. K. Chaudhury and M. J. Owen, J. Phys. Chem. **97**, 5722 (1993); S. Kim, G. Y. Choi, A. Ulman, and C. Fleischer, Langmuir **13**, 6850 (1997); P. Silberzan, S. Perutz, E. J. Kramer, and M. K. Chaudhury, Langmuir **10**, 2466 (1994); P. Attard, J. Phys. Chem. B **104**, 10 635 (2000).